40 Years of Full-scale Infrastructure Testing at a National Geotechnical Experimentation Site: Clay Site.

Jean-Louis Briaud, *Distinguished Professor, Zachry Dpt. of Civil Engineering Texas A&M University, College Station, Texas, 77834-3136, U.S.A.; email: briaud@tamu.edu*

ABSTRACT*: A site at the Texas A&M University RELLIS campus was dedicated to full-scale infrastructure testing in 1978. It was designated as a National Geotechnical Experimentation Site by NSF and FHWA in 1992. The site is made of 12 m of stiff to very stiff clay, within which most experiments took place, and an underlying deep layer of clay shale. The water table is approximately 6 m deep. Over the last 40 years, many full-scale instrumented experiments on infrastructure elements have been conducted at that site. The main projects include grouted anchors, drilled shafts with and without intentional defects, post-grouted drilled shafts, drilled and grouted piles, geothermal piles, soil nails, a pickup truck crashing into a pole founded on a single pile, as well as various mechanical and erosion in-situ tests. Each one of those projects is described and the results and lessons learned from these full-scale infrastructure tests and associated soil tests are reported in this paper; reference to related reports is made for more details on each project.*

KEYWORDS: drilled and grouted piles, grouted anchors, soil nails, post-grouted drilled shafts, defects in drilled shafts, geothermal piles, in-situ tests, laboratory tests, full-scale testing.

SITE LOCATION: Geo-Database

INTRODUCTION

In the late 70s, the need for full-scale testing led the Texas A&M University (TAMU) geotechnical faculty to start the development of two experimental sites on what is now called the TAMU RELLIS campus located 17 km from the main TAMU campus in College Station, Texas. Two sites were identified, one with 12 m of medium dense silty sand and one with 12 m of stiff to very stiff medium plasticity clay. In 1992, after a national competition including about 90 proposals, two primary National Sites were selected jointly by the National Science Foundation and the Federal Highway Administration: one at TAMU and the other at Treasure Island in San Francisco. They were designated as National Geotechnical Experimentation Sites, or NGES. The TAMU-NGES was subdivided into two sites: the clay site and the sand site. This paper deals with the experiments at the clay site, and a companion paper examines the experiments at the sand site. Since 1978, many projects have been conducted at those sites mostly by the author but also by colleagues within the U.S.A. and from other countries. The main projects at the clay site are described in this paper and include grouted anchors, drilled shafts with and without intentional defects, post-grouted drilled shafts, drilled and grouted piles, geothermal piles, soil nails, a pickup truck crashing into a pole founded on a single pile, and various mechanical and erosion in-situ tests. Each one of those projects is described, and the results and lessons learned from these full-scale infrastructure tests and associated soil tests are reported in this paper; also included are references to related reports providing further details on each project.

THE CLAY AND THE SITE GEOLOGY

The stratigraphy of the site is as follows (Fig. 1, Briaud, 1997(a)). The first layer is a clay layer of the Pleistocene Age which was deposited about 200,000 years ago as an overbank sediment; it extends from 0 to 5.5 m depth. The second layer is a layer of sand and gravel also of the Pleistocene Age; it is a channel deposit which has variable thickness with an average of 1 m. The third layer is a clay layer of the Mid-Eocene Age, deposited through a series of transgression and regression of the Gulf of Mexico some 45 million years ago; it is 6 m thick. The underlying layer at the site is a layer of clay-shale also of the Mid-Eocene Age, similarly deposited through a series of transgression and regression of the Gulf of Mexico some 45 million years

Submitted: 1 October 2020; Published: 10 August 2021
Reference: Briaud J.L. (2021). 40 Years of Full-scale Infrastructure Testing at a National Geotechnical Experimentation Site: Clay Site. International Journal of Geoengineering Case Histories, Volume 6, Issue 3, pp. 1-24, doi: 10.4417/IJGCH-06-03-01

ago; it extends to at least 50 m. The clay is over consolidated by desiccation. The average properties of the soil layers are summarized in Figs. 1, 2, and 3. The symbols used in Fig. 1 are the ones commonly used. In Fig. 2, the SPT N values are raw uncorrected values, and the preconsolidation pressures σ'_p were obtained from consolidation tests. The ground water level is found at a depth of 6 m.

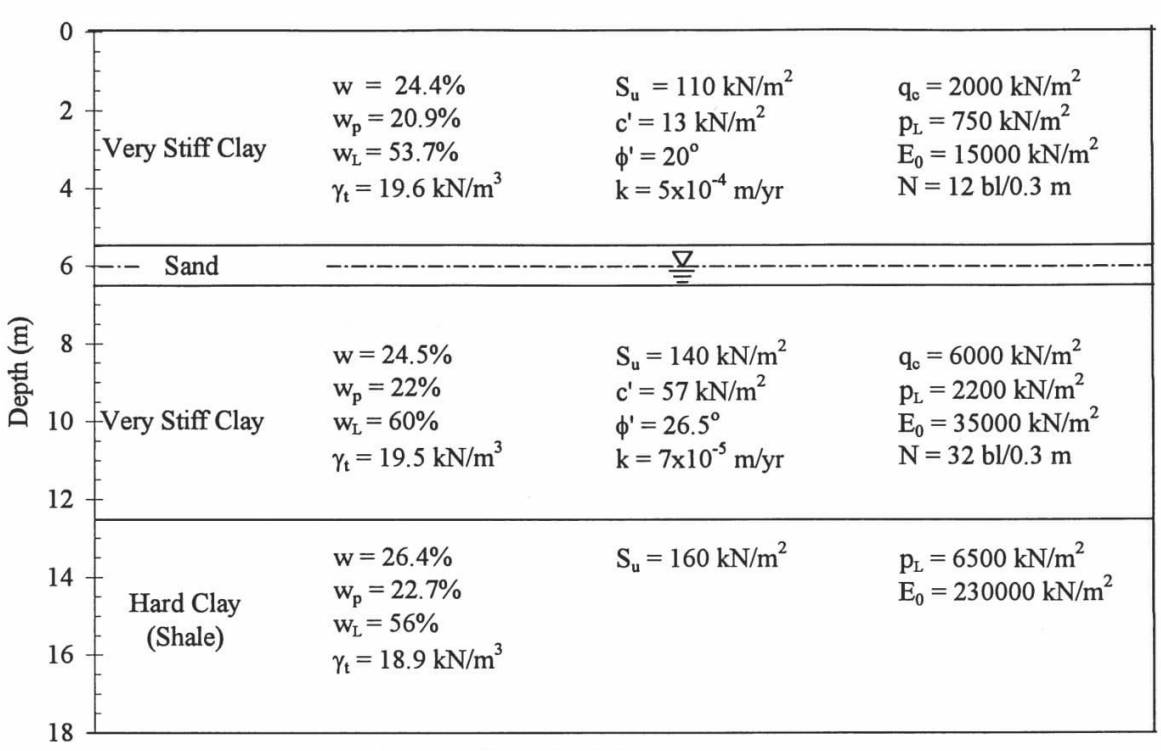


Figure 1. Stratigraphy of the NGES-TAMU clay site (Briaud, 1997(a)).

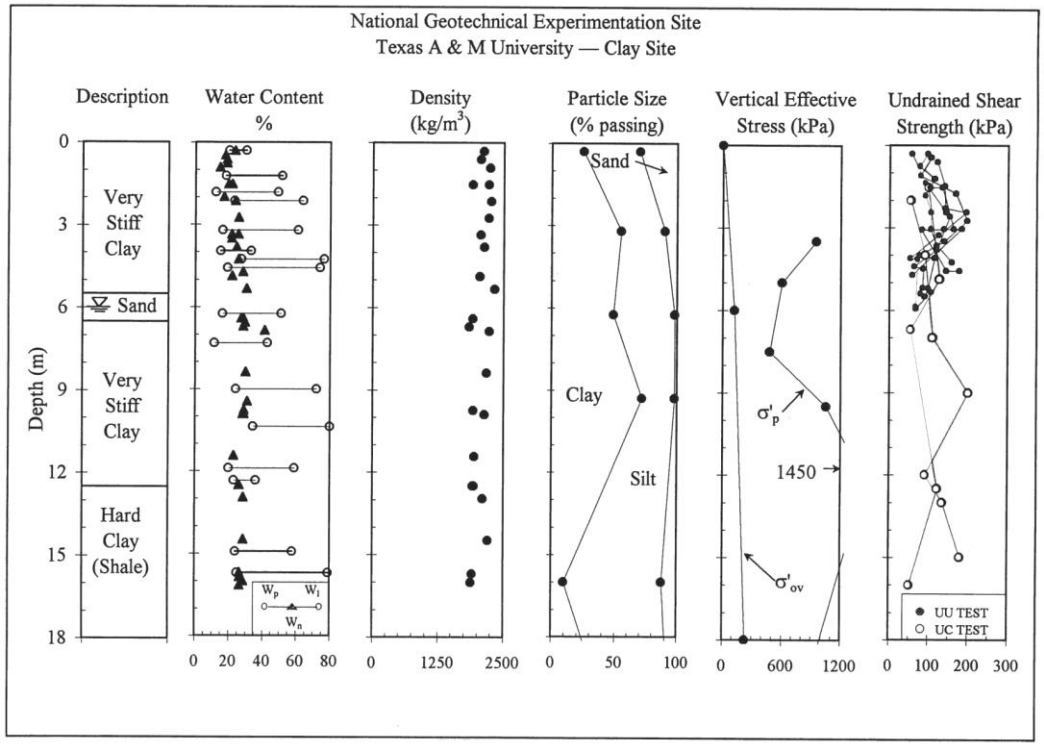


Figure 2. Laboratory test results (Briaud, 1997(a)).

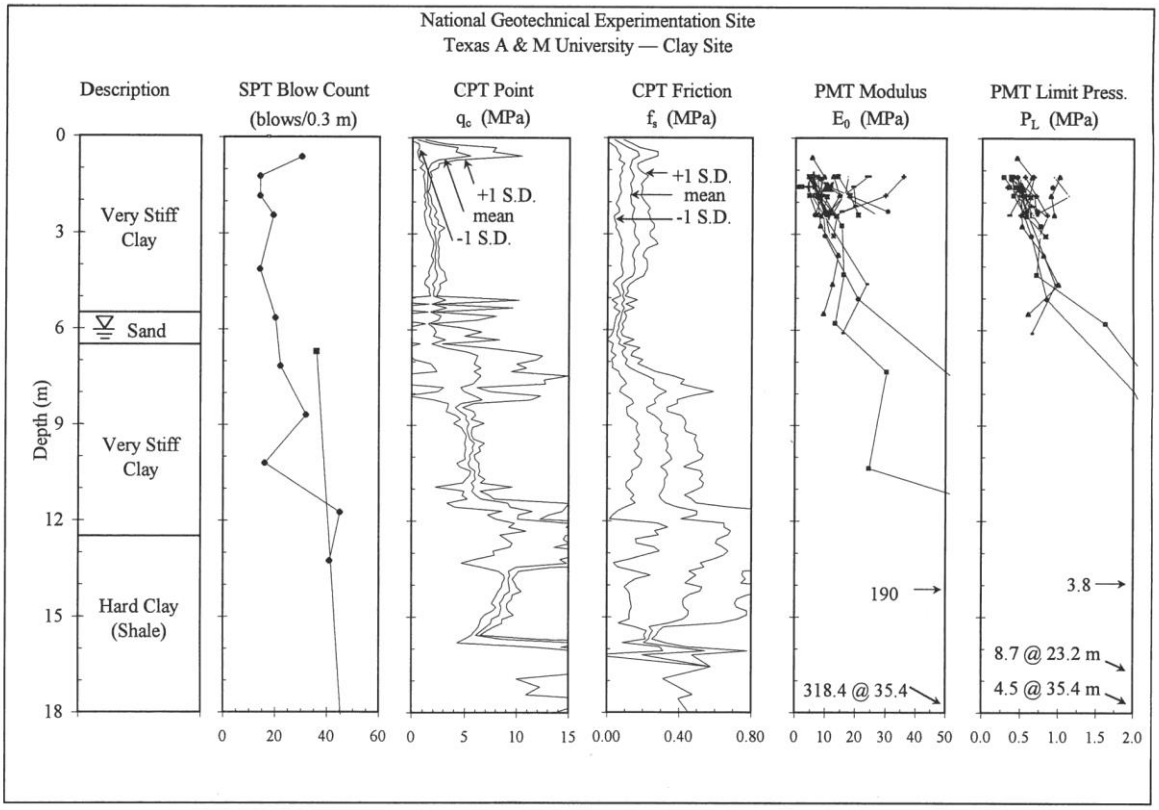


Figure 3. In-situ test results (Briaud, 1997(a)).

THE IN-SITU TESTS

A large number of conventional in-situ tests were conducted at the site, including cone penetrometer tests (CPT), pressuremeter tests (PMT), and standard penetration tests (SPT) with an estimated energy of 55% of maximum energy. The average results are shown in Fig. 3. Some less conventional tests were also conducted; they included the self-boring pressuremeter test and the step blade test (Gan, Briaud, 1987), as well as the borehole erosion test (Briaud, Chedid, 2015; Briaud et al, 2017).

Self-boring Pressuremeter Tests and Step Blade Tests

In 1986, a self-boring pressuremeter unit was used at the site; much was learned about how difficult and time-consuming it is to use such a device. A preboring pressuremeter was also used along with a step blade device (Handy et al., 1982). Some self-boring results were obtained but the unit ended up being destroyed. While the K_o value from self-boring pressuremeter tests tends to be recognized as reliable, one lesson was that the self-boring K_o value depends on the choice of the initial diameter of the inflatable part of the probe during calibration. Indeed, if this initial diameter is smaller than the diameter of the hole created by the self-boring PMT drilling tool, horizontal decompression will take place during drilling followed by recompression during inflation; this likely leads to underestimating K_o. If the initial diameter is larger, the horizontal stress will be higher than at rest; this leads to overestimating K_o. It is not possible to create a probe diameter which is perfectly equal to the diameter of the hole created by the drilling tool because the probe sheath is compressible and the initial diameter of the inflatable part of the probe would have to be set equal to the diameter of the steel tube on the probe below the membrane during penetration at a pressure equal to the K_o pressure, which is unknown.

The step blade test (SBT) was invented by R. L. Handy at Iowa State University (Handy et al., 1982). In 1986, this test was performed at the clay site in tandem with the self-boring and preboring pressuremeter tests mentioned above. The idea of the SBT is to use a blade with steps of increasing thickness and a pressure cell on each thickness (Fig. 4). The pressures read on each blade are plotted versus the blade thickness and extrapolated to zero thickness to obtain the K_o value. This is a very good

idea in theory, but it does not work. The reason, discovered during those tests (Gan and Briaud, 1987), is that the blade is inserted through a penetration process combined with a lateral expansion process created by the increasing thickness of the blades. The lateral expansion leads to increasing horizontal pressures with increasing thickness but further penetration leads to decreasing horizontal pressures. The combination of the two processes leads to data which typically shows an initial increase in pressure for the first two blades and often a lower pressure for the third blade (Fig. 4). This observation skews the extrapolation and leads to K_o values which are typically too high (Fig. 5). The preboring pressuremeter gave K_o values which were close to the self-boring pressuremeter. The horizontal pressure at rest for the preboring pressuremeter was obtained from the early part of the pressuremeter curve (Gan, Briaud, 1987).

Borehole Erosion Test (BET)

This is a test which was developed in 2014 at both the clay and sand TAMU-NGES sites for measuring the erodibility of the soil while drilling a borehole by the wet rotary method (Briaud, Chedid, 2015; Briaud et al., 2017). The borehole is drilled to the depth of interest, e.g., 4 m. The drilling rods are removed and a mechanical borehole caliper is used to record the diameter of the hole as a function of depth, called the diameter profile. The rods without the drill bit are reinserted in the borehole and water is circulated down the rods and up the annulus between the rods and the borehole wall. The water flow is recorded by a flow meter in line with the pump and the flow is maintained for a chosen time, e.g., 10 minutes. Then the rods are removed and the borehole caliper is used to record the diameter of the hole as a function of depth. The increase in radius divided by the flow time is the erosion rate corresponding to the water velocity imparted. By repeating this process for other velocities, the erosion function is described for all soils within the borehole depth. A typical result from a test at the site is shown in Fig. 6. The diameter profile C-0 was the zero-reading profile for the borehole as drilled, profile C-1 was obtained after 10 minutes of water flow at 0.4 m/s, profile C-2 after 10 minutes at 1.36 m/s, and profile C-3 after 10 minutes at 1.19 m/s. The BET has applications to bridge scour, meander migration, dam erosion, levee overtopping, and beach erosion.

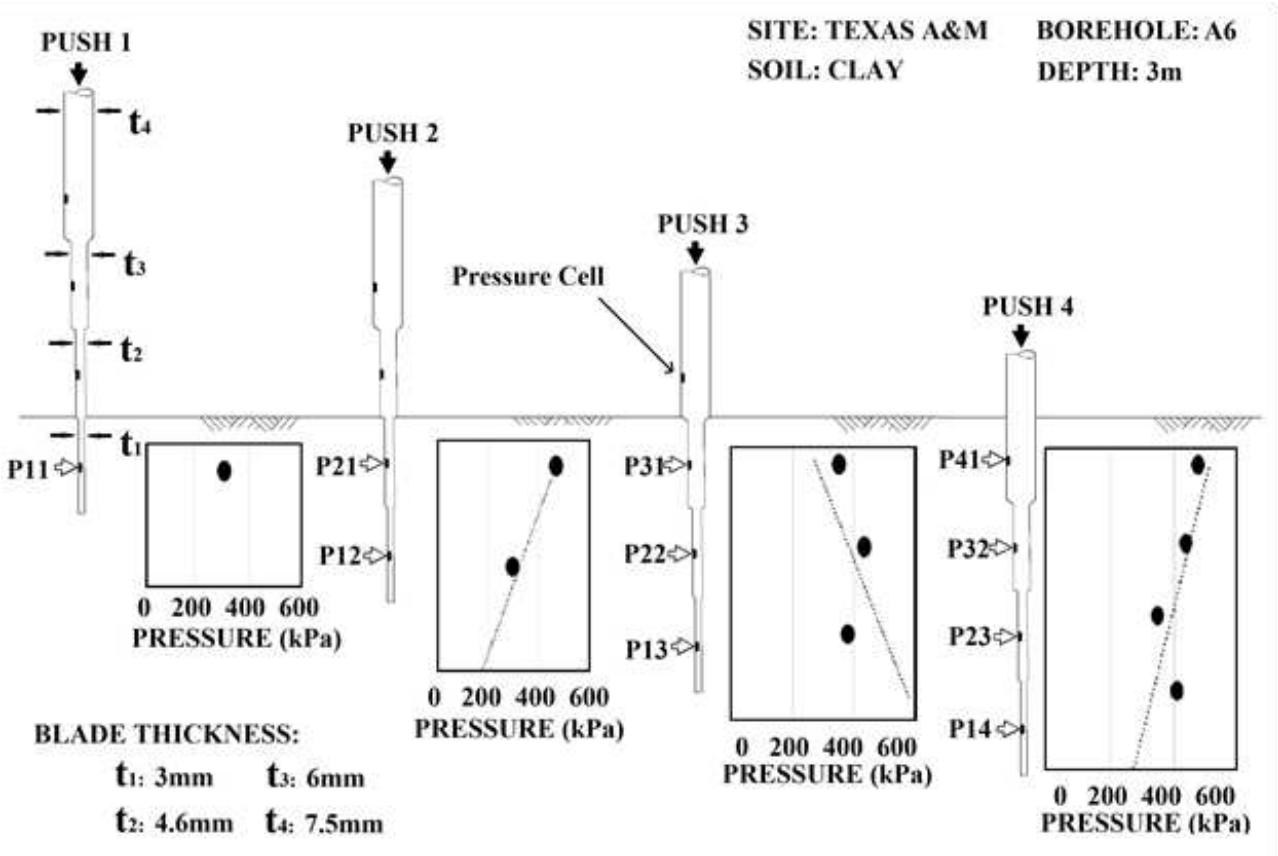


Figure 4. Stepped blade test (after Gan, Briaud, 1987).

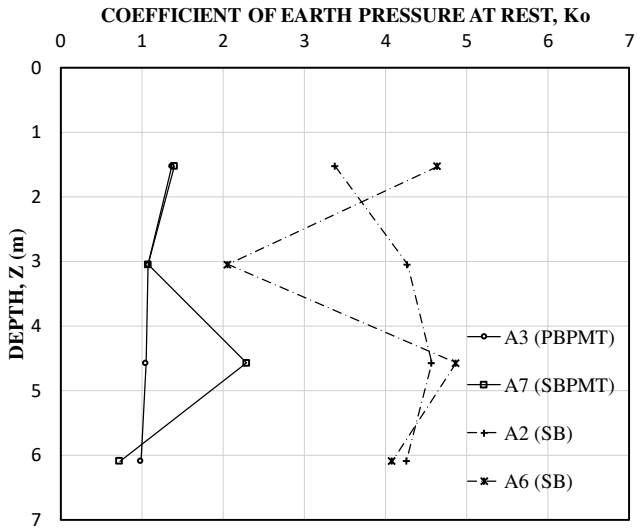


Figure 5. Coefficient of earth pressure at rest from prebored pressuremeter (PBPMT), self-boring pressuremeter (SBPMT), and stepped blade (SB) (after Gan, Briaud, 1987).

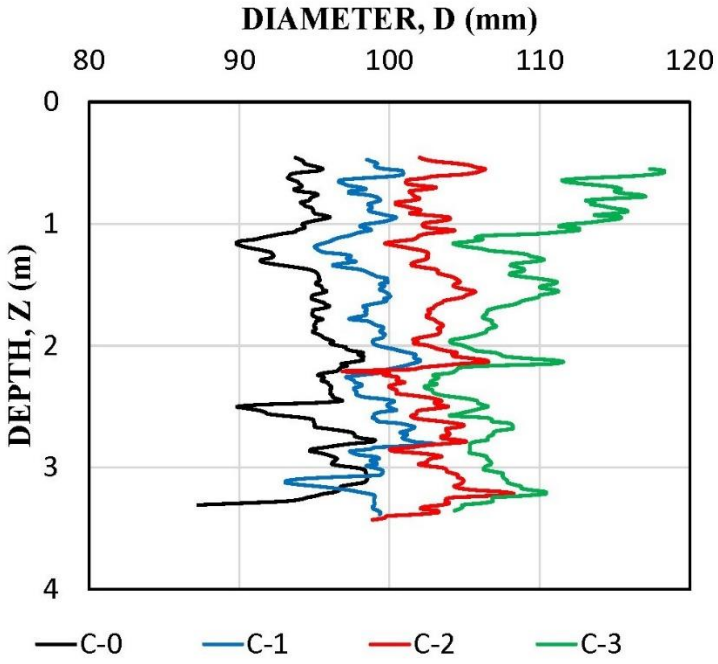


Figure 6. Borehole Erosion Test results (after Briaud et al., 2017).

BORED PILES UNDER MONOTONIC HORIZONTAL LOADING

From 1977 to 1979, lateral load tests were conducted on three bored reinforced concrete piles (Bierschwale et al, 1981). The 1977 bored pile had a diameter D = 0.91 m and a length L = 6.1 m, the 1978 bored pile had a diameter D = 0.91 m and a length L = 4.6 m, and the 1979 bored pile had a diameter D = 0.76 m and a length L = 4.6 m. All lengths refer to the embedded length. The load was applied incrementally at a point 0.79 m above the ground surface. The duration of each load step was 30 minutes for the 1977 and 1978 piles. Two tests were conducted on the 1979 pile; the first one had 30-minute load steps, and for the second one the load steps were kept until very little movement was noticeable. This long-term test lasted 205 days. Measurements of lateral earth pressure at various points along the length of the piles, displacement near the ground surface, and rotation in the plane of loading were obtained for each increment of load. Fig. 7 shows the results of the load

tests on the three piles. The load displacement curves for the tests on the 1979 pile indicate that the difference between the 30-minute load steps and the long-term load steps provides a displacement ratio of about 2. Pressure cells were installed on the piles, and the results for the 1978 pile are shown in Fig. 8. Note that the maximum pressure on the pressure cells aptly matches the limit pressure of the pressuremeter. This observation contributed to the development of the PMT P-y curve method (Briaud et al., 1985), and later to the Simple Analysis for Lateral Load On Piles method (Briaud, 1997(b)).

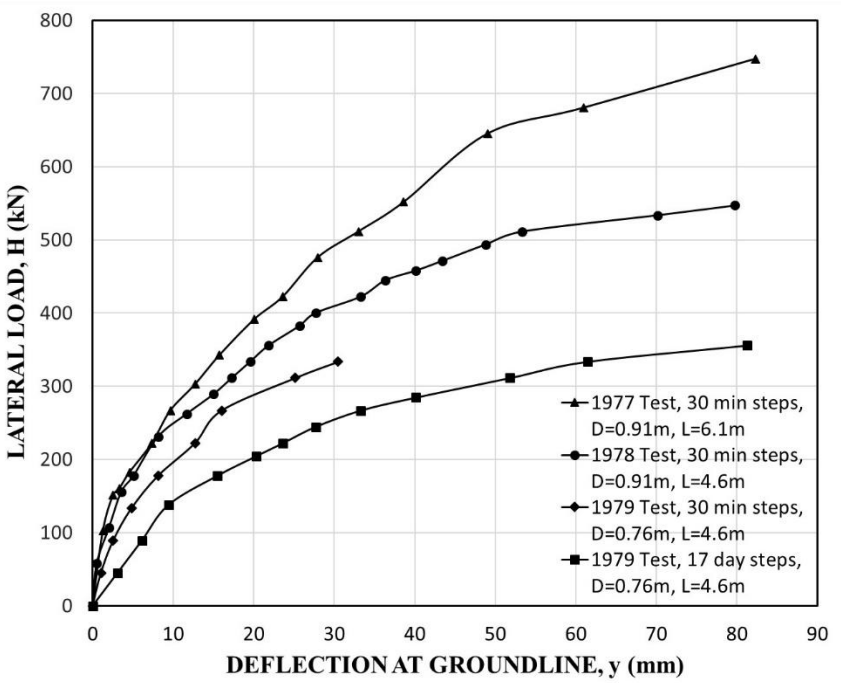


Figure 7. Horizontal load test on 3 bored piles (after Bierschwale et al., 1981).

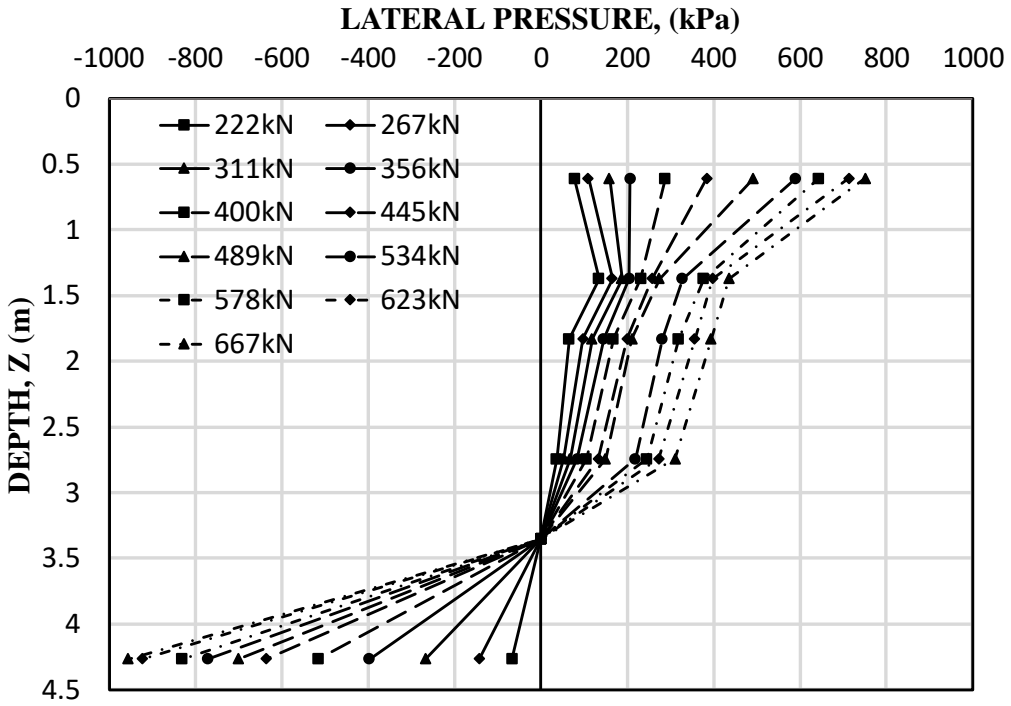


Figure 8. Pressure cell profile for the 1978 pile (after Bierschwale et al., 1981).

DRILLED AND GROUTED PILES UNDER CYCLIC VERTICAL LOADING

Drilled and grouted piles are used offshore and consist of drilling a hole typically by the wet rotary method, lowering a smaller diameter steel casing and grouting the annulus between the borehole wall and the casing. Two drilled and grouted piles were constructed and tested in 1988 (Briaud, Kubena, 1990). The boreholes were drilled with drilling mud, and were 203 mm in diameter and 12.2 m deep. Grout was placed by gravity through a tremie reaching the bottom of the drilled hole; being heavier than the drilling mud, the grout displaced the mud upward. The closed end steel casing was lowered in the open hole, thus displacing the mud from the hole and then squeezing the grout in the annulus; the casings were 127 mm in diameter with a 9.5 mm wall thickness. The steel casings were instrumented with removable extensometers to obtain the load distribution as a function of depth. The tension load tests were carried out in 15-minute load steps and consisted of monotonic loading, including creep as well as cyclic and rate loading (Figs. 9 and 10). A loud noise was heard when the top movement reached 1 mm, likely corresponding to cracking of the grout annulus. The ultimate loads were 1188 kN and 1165 kN for both piles and the ratio of pile-soil interface shear strength to the soil undrained shear strength from unconfined compression tests, often called the α value, was consistently equal or higher than 1.

The piles were extracted after the project was completed and came out with a 10 mm thick layer of clay attached to the grout curtain. This is believed to be due to the hydration of the grout drawing water from the soil and forming a thin layer of hard soil around the pile where the failure occurred. During extraction, it was also observed that some of the grout curtain fell off the pile as slabs of grout. This leads to the question of how well the grout adheres to the pile; evidently, well enough to transfer the soil strength at the interface since α was 1 or above. Nevertheless, shear keys are recommended when using such piles. The rate effect tests confirmed that the power law model for rate effect proposed by Briaud and Garland (1985) is valid (Eq.1) and led to a rate exponent of 0.02 for this stiff to very stiff clay. This value corresponds well with the exponent values measured in special rate effect pressuremeter tests at that site.

$$\frac{Q_1}{Q_2} = \left(\frac{r_1}{r_2}\right)^{n_r} \tag{1}$$

Where Q_1 and Q_2 are the loads corresponding to the same displacement but to rates r_1 and r_2 respectively, and n_r is the rate exponent. The accumulation of creep displacement with time under a sustained load started to be significant after 50% of the ultimate load was reached. The cyclic tests confirmed that the power law model for cyclic displacement accumulation proposed by Briaud and Felio (1986) is valid (Eq.2), and led to a cyclic degradation exponent n_c varying between 0.04 and 0.05 for this stiff to very stiff clay (Figs. 9 and 10). This value corresponds well with the exponent values measured in special cyclic pressuremeter tests at that site.

$$\frac{\Delta_N}{\Delta_1} = N^{-n_c} \tag{2}$$

Where Δ_N and Δ_1 are the displacements at the top of the first and Nth cycles respectively, and n_c is the cyclic exponent.

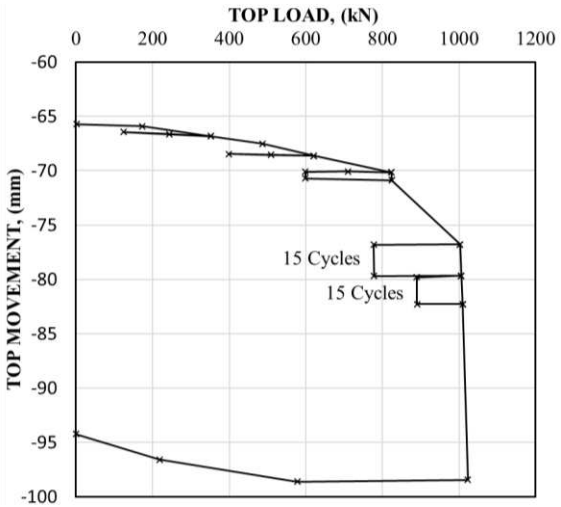


Figure 9. Cyclic and creep tests on drilled and grouted pile (after Briaud, Kubena, 1990).

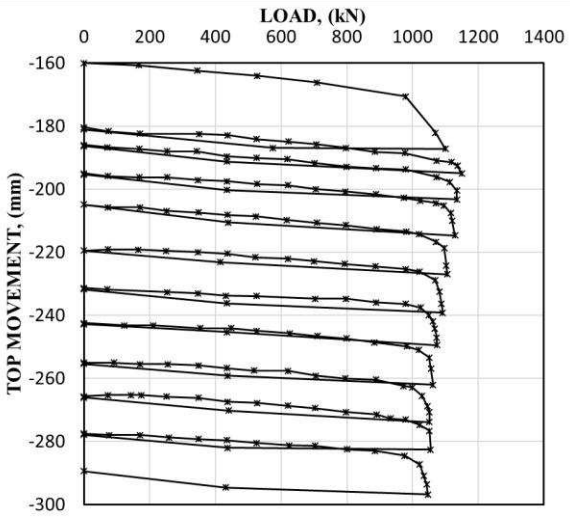


Figure 10. Tension load test on a drilled and grouted pile (after Briaud, Kubena, 1990).

PULLING ON GROUTED PILES FROM THE BOTTOM

Overconsolidated soils such as the one at this site have friction load transfer curves which exhibit post-peak strain softening. During vertical loading, the displacement of an infinitely stiff pile is the same along the entire pile and the peak friction will therefore be mobilized at the same displacement all along the pile. As the pile stiffness decreases, the displacement of the pile is larger at the top than at the bottom, and the friction load transfer curve may be at the post-peak value at the top when it is still at the pre-peak value at the bottom. This averaging effect leads to the conclusion that in overconsolidated soils, the more compressible the pile is, the lower the ultimate capacity will be (Murff, 1980). This is called the length effect.

As learned from the previous project, drilled and grouted piles loaded in tension soon exhibit cracking of the grout curtain. As a result, the stiffness of the pile is reduced and likely leads to a lower ultimate capacity because of the length effect. If, on the contrary, such piles were loaded by pulling the pile from the bottom, the grout would remain in compression, the stiffness of the pile would not decrease during loading, and the ultimate capacity would be higher. This premise was investigated in 1990 by load testing two drilled and grouted piles (Chaouch, Briaud, 1991, 1992). Two 152 mm diameter bored holes were drilled under slurry down to a depth of 12. 2 m. Grout was pumped down to the bottom of the hole by a tremie. Then a closed end steel pipe, 88.9 mm in outside diameter and 6.3 mm thick, was lowered in each one of the two holes, thereby displacing the grout to form the grout curtain. After curing of the grout, the tension load tests were conducted in a series of load steps equal to 40 kN and lasting 15 minutes each. The same series of cycles and rate effect tests were conducted on the two piles. Fig. 11 shows the envelope of the load displacement curves for the two piles.

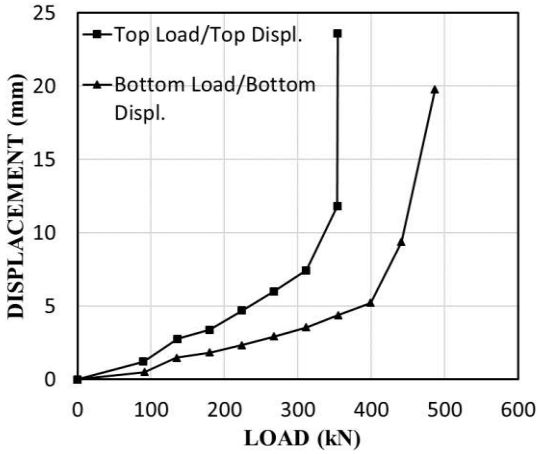


Figure 11. Load displacement curves for the piles pulled from the top and pulled from the bottom (after Chaouch, Briaud, 1992).

The ultimate load of the pile pulled from the top was 355 kN, while it was 490 kN for the pile pulled from the bottom (a 38% increase). The initial slope of the curve or pile stiffness for the pile pulled from the top was 50 kN/mm, while it was 100 kN/mm for the pile pulled from the bottom. Therefore, in this case, the pile pulled from the bottom was 38% stronger and 100% stiffer than the pile pulled from the top. The results of the creep and cyclic tests showed that there was a significant decrease in creep displacement under the same load as well as a significant reduction of accumulated cyclic displacement for the pile pulled from the bottom compared to the pile pulled from the top.

INTEGRITY TESTING OF DRILLED AND GROUTED PILES

This project was undertaken in 1987 to evaluate the ability of oil field grout logging technology to determine the integrity of drilled and grouted piles (Briaud, Dupin, 1990). One drilled and grouted pile was constructed with known defects (Fig. 12). First, a 33.5 m deep hole was drilled dry in the very stiff clay with three different diameter augers. From a depth of 0 to 12.2 m, the hole diameter was 0.91 m; from 12.2 to 27.1 m, it was 0.76 m; and from 27.1 to 33.5 m, it was 0.61 m. The volume of grout necessary to fill the annulus between the hole and the casing up to a depth of 5.6 m below the ground surface was calculated and placed in the bottom of the hole. A 0.51 m diameter closed end casing was lowered into the borehole thus squeezing the grout in the annulus. The wall thickness of the casing was 19 mm. From 0 to 5.6 m, the annulus between the casing and the wall of the hole was filled with loose cuttings of clay. From 5.6 to 12. 2 m, the annulus was left unfilled by creating a 360° empty chamber void made of a larger diameter casing welded to the 0.51 m diameter casing (Fig. 12). From 12.2 to 18.3 m, a 45° vertical channel void was created in the grout curtain (East quadrant). From 18.3 to 26 m, the pile was fully grouted with a 127 mm thick grout curtain. From 26 to 33.5 m, the pile was fully grouted with a 50 mm thick grout curtain.

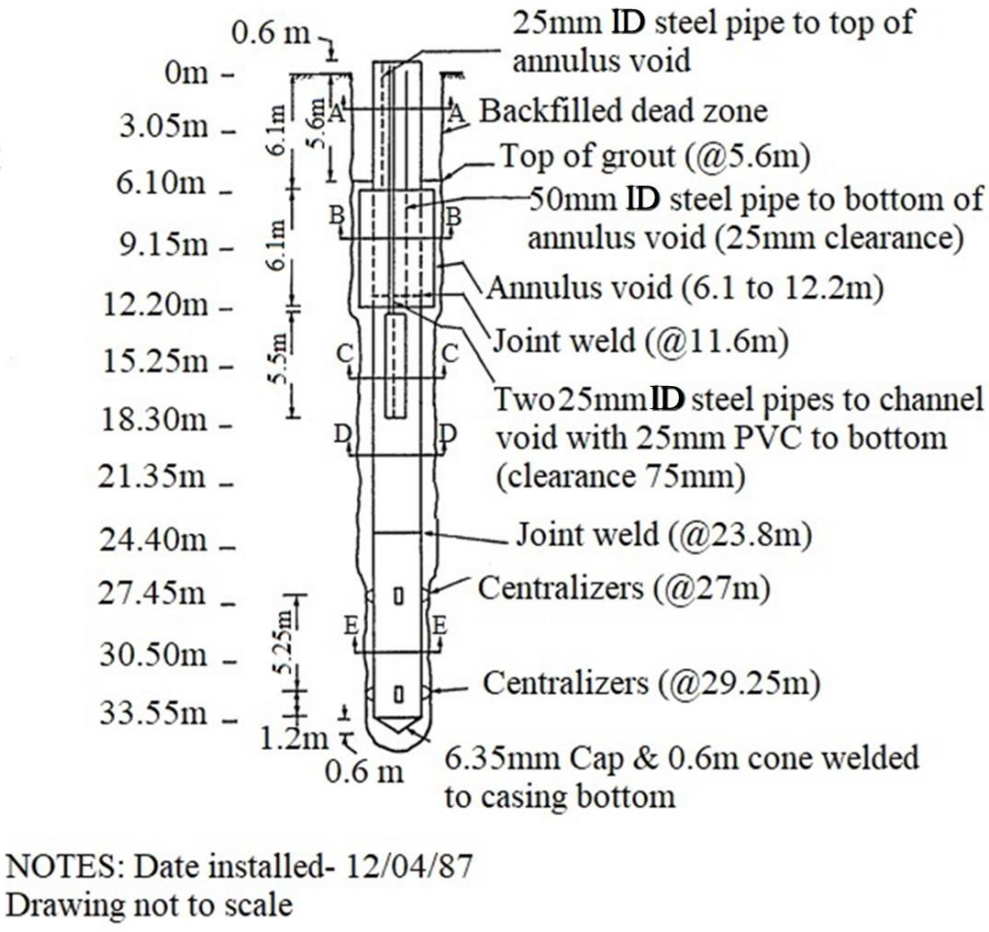


Figure 12. Drilled and grouted pile with defects (after Briaud, Dupin, 1990).

The pile was logged with a series of sonic, ultrasonic, gamma-gamma, and neutron logging tools. The ability of each tool to detect the built-in defect was evaluated. The sonic tools have to be lowered in the interior of the casing with centralizers and the casing must be filled with water. The transmitter emits a 20 kHz compression wave which propagates radially through the water, hits the casing, and travels along the casing. The receiver records the travel time from the transmitter to the receiver and the amplitude of the attenuated wave. Various degrees of attenuation are interpreted as partial grout coverage through calibration. The ultrasonic tools work on the same principle but the wave frequency is 450 kHz. The transmitter is also a receiver, and the waves travels radially to the casing and back to the receiver. The decay of the amplitude as a function of time is related to the compressive strength of the grout curtain.

The gamma-gamma tools are lowered against the wall of the casing with a spring-loaded decentralizer. The source emits gamma rays made of high energy photons, which hit the atoms in the casing and grout curtain; the penetration of the gamma rays is about 100 mm. The denser the material, the larger the number of atoms per unit volume and the smaller the number of photons arriving at the detector. The neutron tools are also lowered against the wall of the casing. The source emits rays of fast neutrons which are best slowed down by hydrogen atoms because they are about the same size. The slow neutrons are counted at the receiver and indicate the water content as well as the porosity of the material penetrated. Neutrons penetrate further than gamma rays, and the neutron tool gives a porosity profile of the grout curtain.

The sonic and ultrasonic tools gave results which were not clear even when the water inside the casing was pressurized to 5.6 MPa. The gamma ray tool delineated very clearly the 360° chamber void and even the narrow vertical chamber void (Fig. 13) but did not detect the change in grout curtain thickness around 27 m. The neutron tool has the potential of penetrating further than the gamma ray tool for very thick casings and grout curtains. Overall, the gamma ray tool worked best.

a. Gamma ray log of North quadrant

b. Gamma ray log of East quadrant

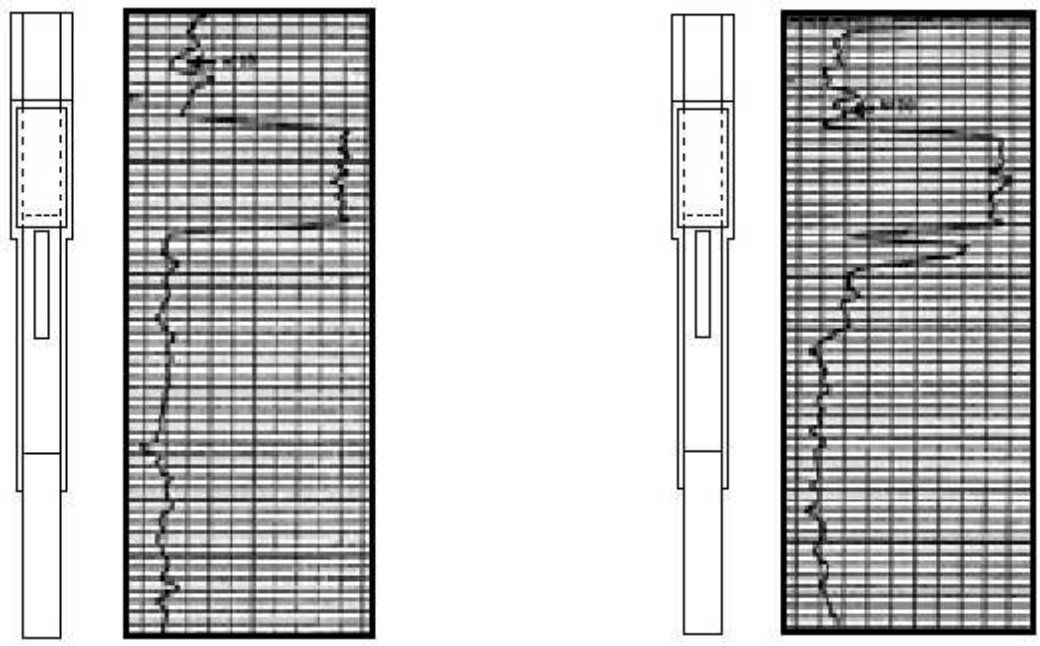


Figure 13. Gamma ray log: a) North quadrant, b) East quadrant (after Briaud, Dupin, 1990).

GROUTED ANCHORS UNDER TENSION LOADING

A set of 10 anchors were installed and tested in tension in 1991 (Powers, Briaud, 1993; Briaud et al., 1998; Fig. 14). First, a borehole was drilled dry to a depth of 13.8 m with a 305 mm diameter hollow stem auger with a detachable point plug. The tendon equipped with centralizers was lowered through the hollow stem to the bottom of the hole. The auger was slowly removed and the point plug stayed at the bottom, while grout was pumped at a pressure of 700 kPa in the annulus all the way to the ground surface. The tendons consisted of seven strands of seven wires each for a total cross section of 980 mm^2 with a guaranteed ultimate tensile strength of 1860 MPa. The tendons of anchors 1 through 6 were sheathed for an unbonded length

from 0 to 9.6 m depth, while anchors 7 to 10 were sheathed for an unbonded length from 0 to 4.6 m depth. For 6 of the 10 anchors, vibrating wire gages were installed on the tendons and embedded in the grout mass.

Different types of load tests were performed on the anchors: proof tests, performance tests, creep tests, and a 70-day load-hold test. The loading history differs for each of those types of tests (Powers, Briaud, 1993). It is common practice to subject every anchor on a project to a proof test, 5% of all working anchors to a performance test, and occasionally to run creep tests. The 70-day load-hold test was specific to this study. An example result is shown for the creep test on anchor 7 (Fig. 15). In a creep test, each load is held for a specific amount of time; this ranges from a few minutes at low loads to up to 300 minutes at 1.33 times the design load. The movement measured at the anchor head was the total movement, including the elastic movement (mostly due to the elasticity of the tendon in the unbonded length) and the residual movement (mostly due to non-recoverable movement and to the change in effective unbonded length when the grout is cracking). The residual movement is the movement read after unloading the anchor; the elastic movement is the difference between the total movement and the residual movement.

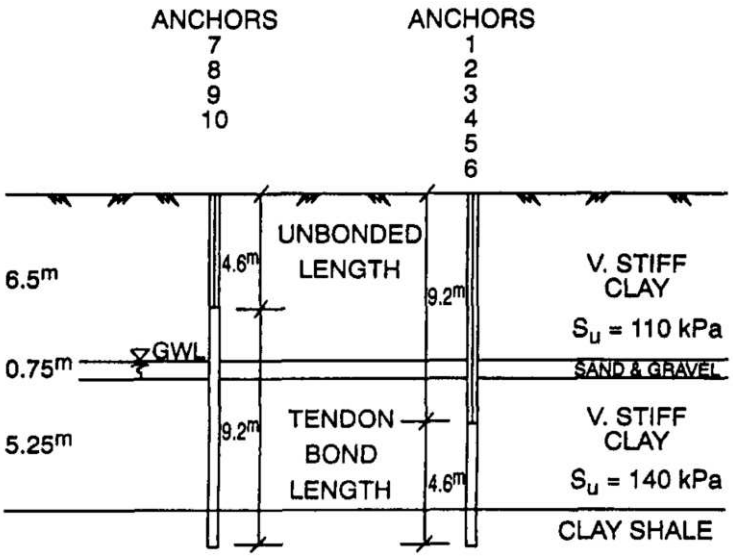


Figure 14. Configuration of the 10 anchors tested (Powers, Briaud, 1993).

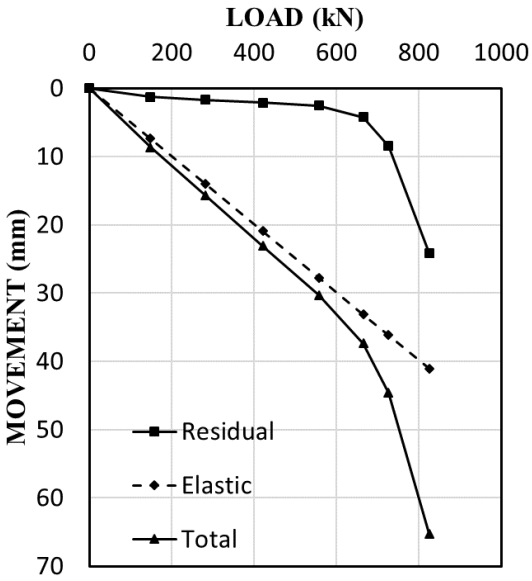


Figure 15. Load movement curve for the creep test on Anchor 7 (after Powers, Briaud, 1993).

The ultimate anchor capacity is defined as the load corresponding to a residual movement of B/10, where B is the anchor diameter. Table 1 shows the ultimate loads for all anchors. The ultimate load for the anchors with a short-bonded length was 23% larger on the average than the ultimate load for the anchors with a longer bonded length. This finding is consistent with the findings of the previous project on drilled and grouted piles where the length effect had been demonstrated. Indeed, the anchors with short unbonded length have a longer length of grout in tension thus cracked, while the anchors with long unbonded length have a shorter length of grout in tension thus less cracked. The cracking of the grout reduces the stiffness and exaggerates the length effect described previously (Murff, 1980). For this reason, an anchor with a short-bonded length carries more load than the same anchor with a long-bonded length. Anchors 1, 2, 7, 8, and 10 were retested to failure in 2013, 22 years after the first tests (Table 1, Sanchez et al., 2017). The average capacity in 2013 was 1.56 times the capacity in 1991.

Table 1. Ultimate loads for the 10 anchors (after Sanchez et al., 2017).

Anchor number	Ultimate load (kN)		Bonded anchor length (m)	Friction stress at failure (kN/m^2)		α values (average over depth)	
	1991	2013		1991	2013	1991	2013
1	867	1348	4.57	65.9	102.5	0.53	0.82
2	1080	1379	4.57	82.1	104.8	0.66	0.84
3	ID[a]	-	4.57	-	-	-	-
4	934	-	4.57	71.0	-	0.57	-
5	ID[a]	-	4.57	-	-	-	-
6	712[b]	-	4.57	54.1	-	0.43	-
7	801	1446	9.15	60.9	109.9	0.49	0.88
8	747	1272	9.15	56.8	96.7	0.45	0.77
9	ID[a]	-	9.15	-	-	-	-
10	801	1272	9.15	60.9	96.7	0.49	0.78

a. Insufficient displacement.
b. Installation difficulties encountered; 60% of anchor not grouted under pressure, just free-fall.

Many other aspects of anchor behavior were studied in this project, including the load distribution in the tendon and in the grout of an anchor, the ratio between the maximum skin friction values f_{max} and various soil properties, the creep rate and the creep load threshold, and the load loss during a 70-day load-hold test. For f_{max}, the following average ratios were obtained:

$\alpha = f_{max}/s_u = 0.52$; $f_{max}/q_c = 0.016$; $f_{max}/p_L = 0.043$; f_{max}(kPa)/N(bpf) = 2.9

where s_u is the undrained shear strength, q_c is the cone penetrometer point pressure, p_L is the pressuremeter limit pressure, and N is the Standard Penetration Test blow count in blows per foot. These ratios are for the tests in 1991. The tests in 2013 showed that the α value went up from 0.52 in 1991 to 0.80 in 2013. Creep movement was found to be excessive (more than 2 mm per log cycles) when the load exceeded 85% of the ultimate load. The creep movement was 2.8 times less for the anchors with short-bonded length than for the anchors with long-bonded length. The load loss test was performed because of concerns that creep in clay might lead to significant load loss over time. The load loss of four anchors locked off for 70 days at a load equal to about half the ultimate load averaged 0.9% of the load per log cycle of time. This corresponds to less than 7% of load loss over 100 yrs.

NON-DESTRUCTIVE TESTING OF DRILLED SHAFTS WITH DEFECTS

Four drilled shafts were built by the A.H. Beck Foundation in 1991 (Ballouz et al., 1991; Briaud et al., 2002). The diameter, length, and defect location and size are shown in Fig. 16. The defects were made of sealed sand bags attached to the reinforcing cage. Five Non Destructive Testing (NDT) companies were invited to come and run their NDT tests and make blind predictions of the length of each pile as well as the location and size of the defects. The methods used were Sonic Echo (SE), Impulse Response (IR), Impedance Logging (IP), and Sonic Logging (SL). The success rate in predicting the length of the piles was gaged in three categories: within + or – 5%, within + or – 15%, and not within + or – 15%. The results are

shown in Fig. 17. The success rate in predicting the location and size of the defects was gaged in three categories: good prediction, fair prediction, and poor prediction. Good prediction meant that the type of defect was well defined and the location was within + or – 0.6 m. Fair prediction meant that the type identified was ambiguous and the location was within + or - 1.8 m. Poor prediction meant the type and location were not detected.

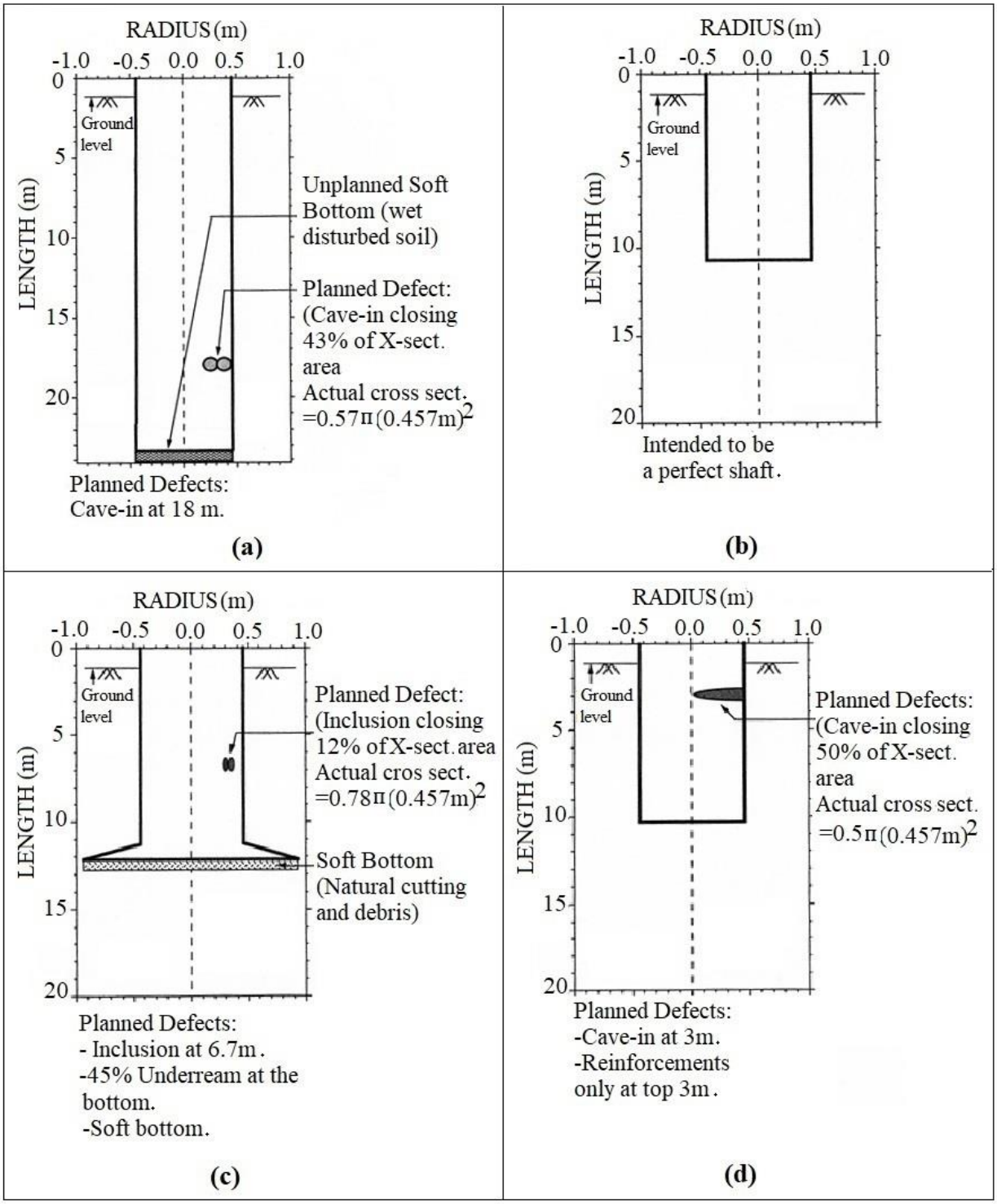


Figure 16. Four drilled shafts with planned defects (a) Shaft 6, (b) Shaft 7, (c) Shaft 8, and (d) Shaft 9 (after Ballouz et al., 1991).

Site (1)	Pile Number (2)	Actual Length (m) (3)	ON SITE A (4)	ON SITE B (5)	ON SITE C (6)	ON SITE D (7)	ON SITE E (8)	SE C (9)	SE D (10)	SE E (11)	IR A (12)	IR B (13)	IR C (14)	IR D (15)	IL A (16)
SAND	1	16.6	●	○	●	◒	●	●	●	●	●	○	●	●	●
	2	11.6	●	●	●	●	●	●	◒	●	●	●	●	●	●
	3	16.5	●	○	◒	●	●	●	●	●	●	●	●	●	●
	4	11.4	-	-	-	-	-	-	-	-	-	-	-	-	-
	5	16.8	○	○	○	○	○	●	○	○	●	◒	○	○	○
CLAY	6	24.1	●	○	●	○	○	◒	○	○	◒	○	◒	○	●
	7	10.7	-	-	-	-	-	-	-	-	-	-	-	-	-
	8	12.2	●	●	●	◒	◒	●	●	●	●	●	●	◒	●
	9	10.4	●	●	◒	◒	◒	◒	●	◒	●	●	◒	●	●
Percent Success			86%	43%	71%	50%	57%	86%	64%	64%	93%	64%	71%	64%	86%
Average			61%					71%			73%				86%

On Site - Predictions made on site, the day of the test, before access to the PVC pipes was allowed.
SE, IR, IL - Final predictions made by Sonic Echo (SE), Impulse Response (IR), Impedance Logging (IL)
A,B, C, D, E -Letters identifying the predicting company
● - Length predicted within ±5%
◒ - Length predicted not within ±5%, but within ±15%
○ - Length not predicted within ±15%

Figure 17. Success rate for predicting the length of the drilled shafts (Briaud et al. 2002).

The results are shown in Fig. 18. In the process of predicting the defects, a number of defects were predicted to exist and did not exist according to the construction record; this is referred to as a false negative. Fig. 19 shows the false negatives. In addition, drilled Shaft 7 was subjected to a conventional static load test, a Statnamic test, and a pile driving test. The results can be found in Briaud et al. (2000) and in Ballouz et al (1991).

Site (1)	Pile No. (2)	ACTUAL DEFECTS: Type and Size (as % of Area) (3)	ACTUAL DEFECTS: Location from top (m) (4)	SONIC ECHO C (5)	SONIC ECHO D (6)	SONIC ECHO E (7)	IMPULSE RESPONSE A (8)	IMPULSE RESPONSE B (9)	IMPULSE RESPONSE C (10)	IMPULSE RESPONSE D (11)	SONIC LOGGING A (12)	SONIC LOGGING C (13)	IMPEDANCE LOGGING A (14)
SAND	1	Bulging (+20%) (U) Necking (-70%)	2.0 - 4.0 5.6	● ○	● ●	● ○	● ●	● ○	● ○	○ ●	◒ ●	◒ ●	● ●
	2	Mud Cake (15 mm) Tremie Displ. (100%) Necking (-45%) (U) Soft Bottom (100%)	0 - 11.6 5.3 5.0 11.6	○ ○ ◒ ●	○ ○ ◒ ○	○ ○ ● ○	○ ● ● ○	○ ○ ◒ ●	○ ○ ◒ ●	○ ○ ● ○	○ ● ○ ○	○ ○ ○ ○	○ ● ○ ○
	3	Underream (+450%) Side Failures (Bulging +100%) (U) Soft Bottom (Sawdust 100%)	5.6 3.0 - 8.0 16.5	● ● ○	● ● ○	● ● ○	○ ◒ ○	○ ● ○	○ ● ○	○ ○ ○	○ ○ ○	○ ○ ◒	● ● ○
	4	Bulging (+30%) (U)	1.2 - 7.5										
	5	Necking (-63%) Bulging (+20%) (U) Bulging (+20%) (U) Soft Bottom (Cuttings 100%)	8.7 3.0 - 8.0 11.5 -14.0 16.8	○ ● ◒ ○	○ ● ○ ○	○ ● ○ ○	● ◒ ○ ○	◒ ○ ● ○	○ ● ◒ ○	○ ○ ○ ○	● ○ ○ ○	◒ ○ ○ ○	● ● ● ○
CLAY	6	Necking (-43%) Soft Bottom (100%)	18.0 24.1	● ○	○ ○	○ ○	○ ○	● ○	◒ ●	○ ○	● ◒	● ●	● ○
	7	No Defect											
	8	Inclusion (-12%) Underream (+450%) Soft Bottom	6.5 12.2 12.2	● ○ ●	○ ○ ○	○ ● ○	○ ○ ○	○ ◒ ○	● ○ ○	○ ○ ○	● ○ ○	● ○ ○	○ ● ○
	9	Necking (-50%)	3.0	○	●	●	●	●	○	●	●	◒	●

● - Good Prediction: Type well defined and location within ±0.6 m
◒ - Fair Prediction: Type ambiguous and location within ±1.8 m
○ - Poor Prediction: Type and location undetected
(U) - Unplanned Defect
A, B, C, D, E - Letters identifying the predicting companies

Figure 18. Success rate for predicting the type and location of the defects (Briaud et al. 2002).

Site (1)	Pile No. (2)	Company A (3)	Company B (4)	Company C (5)	Company D (6)	Company E (7)
SAND	1		Cave-in (17.4 m)			
	2					
	3	Necking (6.0 m)	Necking (6.1 m) Bell (9.7 m)	Necking (12. 6 m)	Necking (7.3 m)	
	4			Necking (5.4 m)		Necking (5 m)
	5			Necking (4.8 m)		
CLAY	6	Bulb (3.2 m) Necking (9.5 m)	Bulb (2.7 m) Necking (10.4 m)	Defect (10.4 m)	Necking (4.3 m) Necking (10.4 m)	
	7	Bulb (2.3 m) Soft bottom	Small bulb near top	Soft bottom		
	8	Bulb (2.1 m)		Defect (2.6 m)	Bulb (2.7 to 3.7 m)	
	9	Soft bottom	Bulb (4 m) Necking (10 m)	Bulb (3.2 m)	Bulb (5.5 m)	

Figure 19. Predicted defects where none existed according to the construction records (Briaud et al. 2002).

POST GROUTED DRILLED SHAFTS

This 2005 project was sponsored by Synchropile to evaluate the increase in capacity brought about by post grouting drilled shaft tips in clay (King et al., 2009, 2015). It consisted of building three drilled shafts: one post grouted drilled shaft (PGDS), one PGDS with a bottom O'Cell, and one regular drilled shaft without post grouting. All three drilled shafts were then load tested to failure. The shafts were instrumented and had a 0.76 m nominal diameter and a length of 10 m. During post grouting, the grout pressure reached 400 kPa and the top of the shaft moved up 5 mm. The load tests were carried out in general accordance with the quick load procedure of ASTM D1143. The load-deflection curves of Fig. 20 show that the ultimate capacities for the PGDS and the conventional drilled shaft are 2323 kN and 2033 kN, respectively. This represents an axial load capacity increase of 14.3%. Similarly in Fig. 20, we can compare the axial loads required to produce a 25 mm top settlement in each case. This top settlement was reached at axial loads of 2217 kN and 1928 kN for the PGDS and conventional drilled shaft, respectively. This demonstrates that for a top deflection of 25 mm, an axial load about 15% higher could be used for the PGDS compared to the conventional drilled shaft. This is due to the fact that the post grouting process prestresses the drilled shaft against the soil, thereby limiting the amount of movement necessary to engage the soil response.

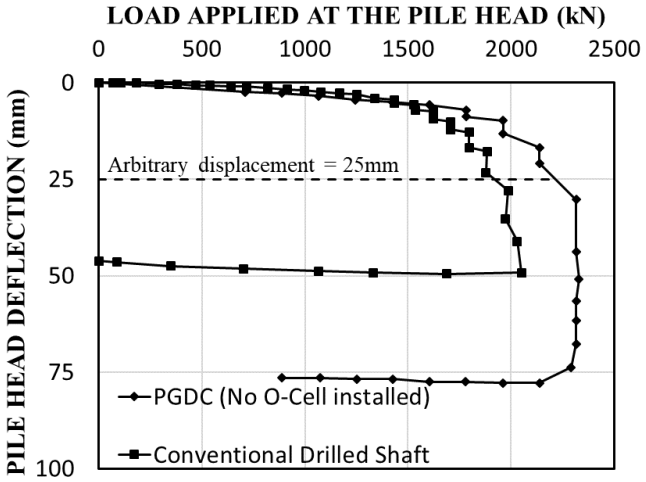


Figure 20. Load settlement curve for conventional and post grouted shafts (after King et al., 2015).

CREEP OF SOIL NAILS

This 2013 project was undertaken because of concerns that in high plasticity clays, soil nails may creep and be unreliable reinforcement (Sanchez et al., 2017). A total of 16 nails were constructed by first drilling a 178 mm diameter hole with a hollow stem auger while collecting Shelby tube samples. The embedded length of the nails varied from 3.05 m to 5.95 m. Grout was poured in the hole and a 25 mm diameter rebar with centralizers was lowered in the hole. The length of grout in contact with the soil varied from 2.1 m to 5 m. The load was applied typically in 22 kN load increments, and the ultimate load ranged from 133 kN for the 2.1 m grouted length nail (NS1) to 311 kN for the 5 m grouted length nail (N1). The load displacement curves are shown for these two nails in Figs. 21 and 22.

As for the anchors' load displacement curves presented earlier, three components of the movement are indicated: total, elastic, and residual. Each load level was held for 10 minutes while recording displacement vs. time. Then the displacement was plotted vs. log of time, and the slope of the line was obtained and defined as the creep rate (mm/log cycle of time). This creep rate is shown for nails NS1 and N1 in Figs. 23 and 24. The allowable creep rate value for nails in common practice is 2 mm per log cycle of time. Figs. 23 and 24 indicate that the nails in this high plasticity stiff clay exhibited an acceptable creep rate until the load level was over 80% of the ultimate load.

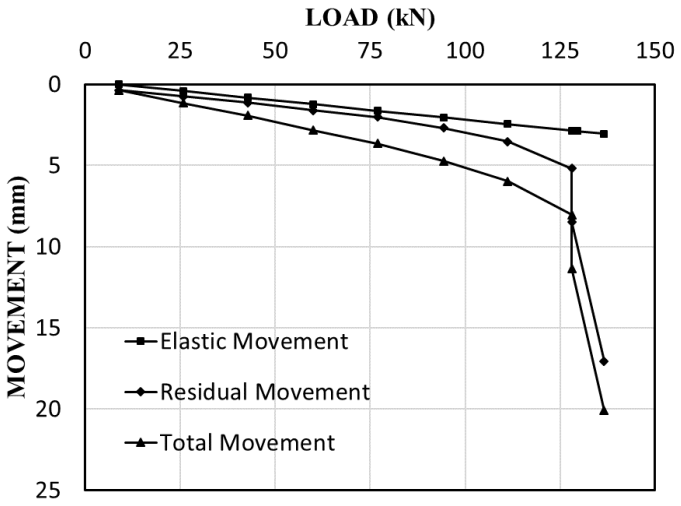


Figure 21. Load test results for nail NS1 (after Sanchez et al., 2017).

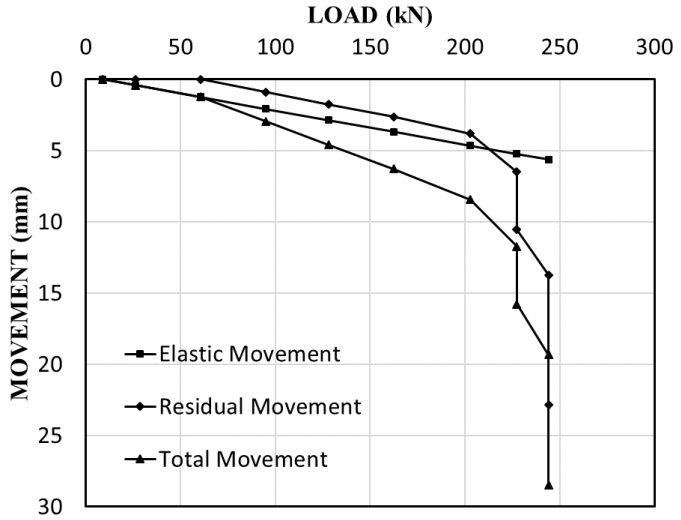


Figure 22. Load test results for nail N1 (after Sanchez et al., 2017).

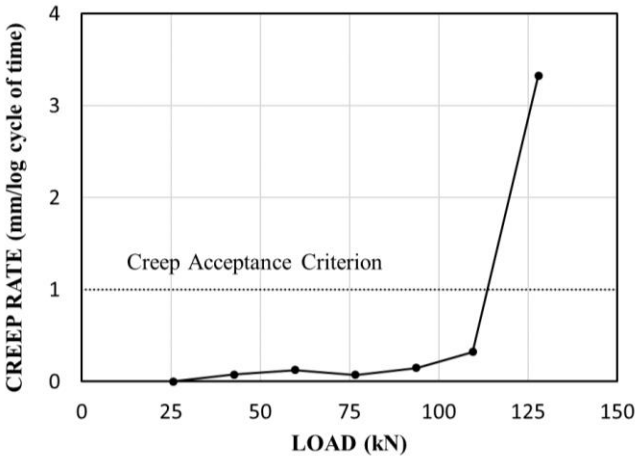


Figure 23. Creep rate for nail NS1 (after Sanchez et al., 2017).

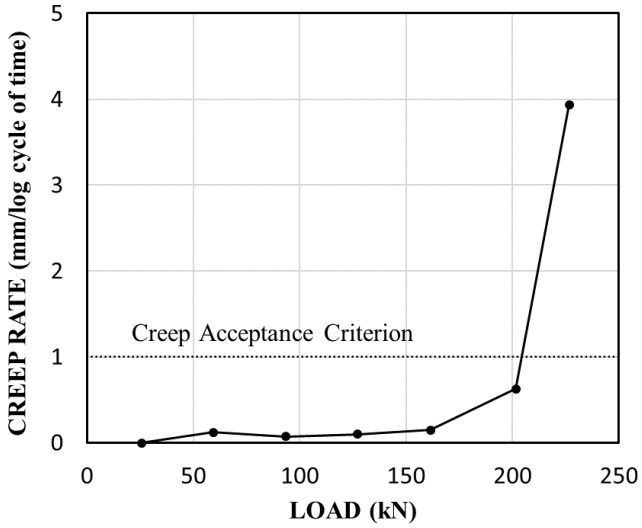


Figure 24. Creep rate for nail N1 (after Sanchez et al., 2017).

Other findings during this project included the fact that the capacity of the same nail was on average 25% higher during the dry season than during the wet season. Also, the creep rate was found to be lower after cyclic loading as long as the creep load applied was below the peak cyclic load. The measured strains indicated that very early during the loading, the strains in the nail are higher than the cracking strain of the grout (100 x 10^{-6} m/m), and therefore the stiffness of the nail is equal to the stiffness of the steel bar.

GEOTHERMAL PILES

Geothermal piles are piles equipped with water loops and used to improve the efficiency of the heating and cooling systems of civil engineering structures. The water circulates in the loops embedded in the piles to benefit from the temperature of the soil as a heat source in the winter and as a cooling source in the summer. These systems have been shown to decrease energy consumption compared to conventional systems, but the impact on the pile behavior of circulating water at a temperature significantly different from the surrounding soil temperature is still being evaluated. This was the purpose of these pile tests (Akrouch, 2014). Two 5.5 m deep and three 3 m deep grouted bored piles were constructed by first drilling dry a 180 mm diameter borehole. Next, a U-shape polyethylene loop made of 25 mm tubing was attached to a 25 mm diameter steel bar equipped with centralizers. The assembly was lowered in the open hole full of grout. The pipe legs of the U were 100 mm apart. The steel bar was instrumented with strain gages and thermocouples. In addition, the relative humidity and temperature of the air were recorded during the tests.

The load test consisted of first applying a chosen load on the pile, keeping that load constant for one hour without any water circulation, and recording the pile head movement as a function of time. Then the same load was kept constant, and water was circulated in the pile for 4 hours at a measured temperature between 10 and 15° C warmer for some piles and 10 to 15° C cooler for other piles than the ambient soil temperature and recording the pile head movement as a function of time. Then the pile was unloaded, and the water circulation was stopped for 19 hours; afterwards, the same sequence was repeated under a higher load. Note that the temperature recorded in a borehole 0.5 m away from the pile did not show any significant temperature variation (less than 1° C). Fig. 25 shows the pile temperature as a function of time, including the constant temperature during the first loading with no water circulation, followed by the temperature of the water during heated water circulation and under the same load.

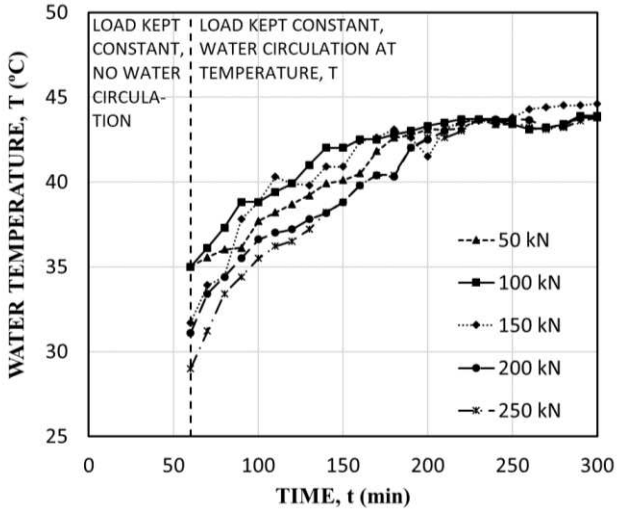


Figure 25. Temperature in water loop inside pile during load test (after Akrouch, 2014).

Fig. 26 shows the air temperature and relative humidity as a function of time during the testing period. Fig. 27 displays the pile top displacement vs. log time, and Fig. 28 illustrates the creep exponent (Eq. 1) for the case of no water circulation (first 60 minutes) and for the case of hot water circulation (next 4 hours). The lessons learned from these experiments were:

1. There is an increase in the rate of creep settlement when the pile is heating the soil and an associated decrease in stiffness. This stiffness decrease can be included in the settlement calculations by using the power law creep rate model (Eq. 1, Akrouch, 2014).
2. There is a decrease in the rate of creep settlement when the pile is cooling the soil and an associated increase in stiffness.
3. There is no indication of a change in ultimate capacity due to the pile heating the soil.
4. There is a slight change in stress distribution in the pile due to the thermal load, but it is minimal overall.

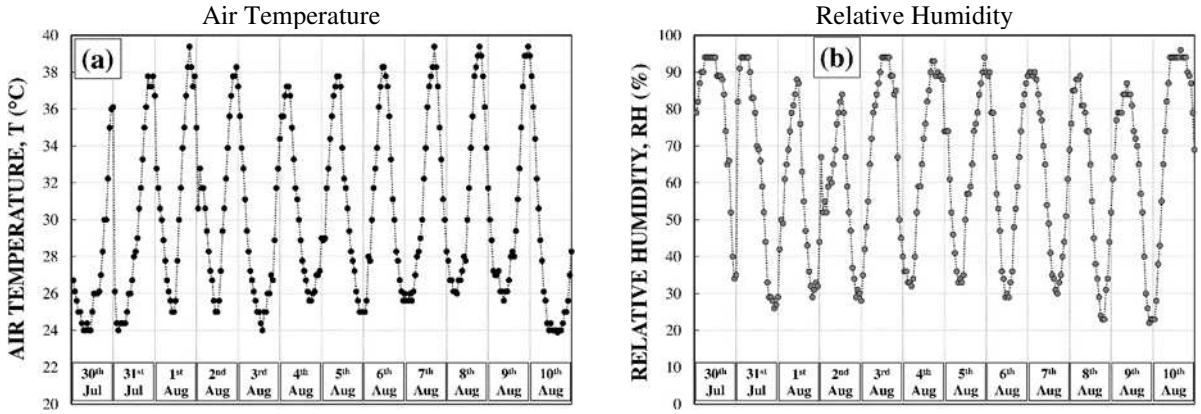


Figure 26. Air temperature and relative humidity during the test of Fig. 26 (after Akrouch, 2014).

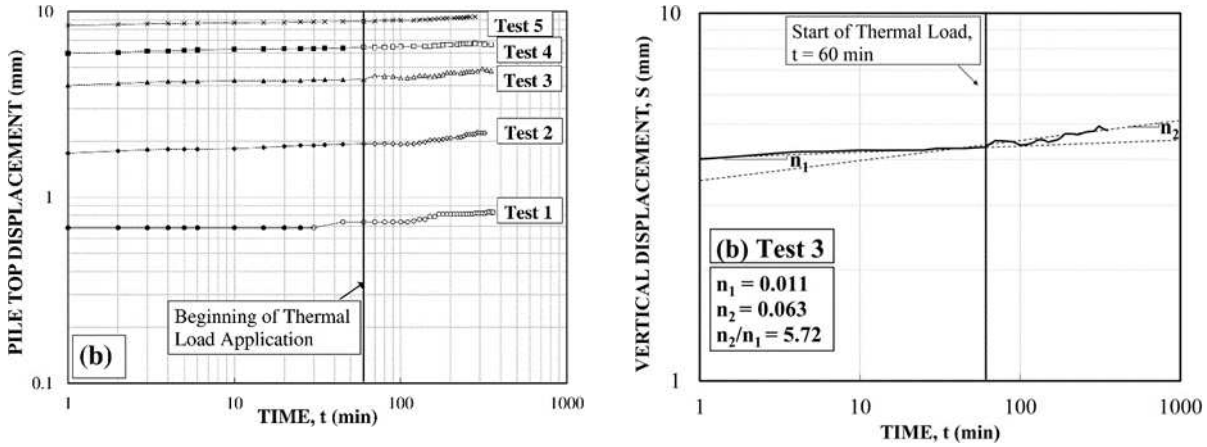


Figure 27. Pile top displacement vs. log time (after Akrouch, 2014).

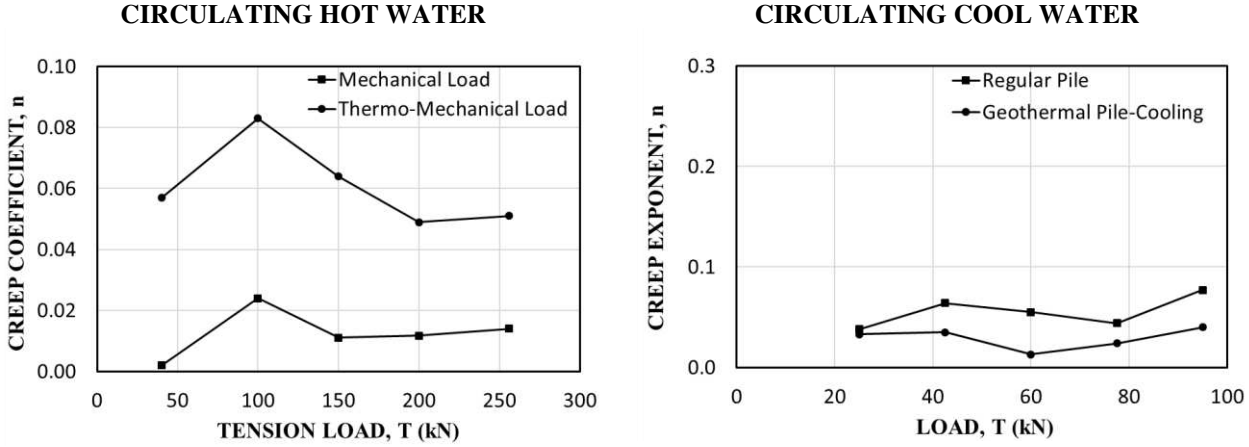


Figure 28. Creep exponent with and without hot water circulation (after Akrouch, 2014).

TRUCK IMPACT TEST ON BARRIERS FOR EMBASSY PROTECTION

Many different types of barriers are used to protect embassies and other critical structures against truck impact. Such an impact generates significant dynamic horizontal loading. A pile foundation is one of the solutions used to anchor the barrier and resist the shock, especially when there is limited right of way. This project performed in the mid-2000s consisted of conducting full-scale tests of truck impact on piles, performing many numerical simulations, and reducing the results into a set of design charts. The work is summarized in three Ph.D. dissertations (Lim, 2011; Mirdamadi, 2014; Pajouh, 2015).
An example of the full-scale tests is shown in Fig. 29. In this test, the pile was a 0.35m diameter steel tube with a 12.7mm wall thickness embedded 2 m in the stiff clay with a pressuremeter limit pressure of about 1100 kPa (Fig. 30). Because the clay soil was very hard, the 0.35 m diameter pile was pushed in a 0.30 m diameter predrilled hole. The truck had a mass of 2300 kg and impacted the pile at 96.5 km/h. The time to reach the peak force of about 400 kN was 0.1 seconds and the corresponding peak displacement was 0.13 m. The truck came to rest after 0.5 seconds and a maximum displacement of the pile of 0.82 m.

The impact force was obtained by using a 3D accelerometer mounted on the bed of the truck behind the cab and by calculating the mass of the truck (F = ma). The movement of the pile was obtained by image analysis using cameras with video capture in three perpendicular directions. A static test was performed on a separate but identical pile a few meters away from the impact test; the load was increased in equal 10-minute long load steps for a total time to failure of 160 minutes. The force vs. displacement curve for the static test and for the impact test are shown in Fig. 30; it indicates that the peak dynamic force is about 3 times larger than the peak static resistance. Numerical simulations using LS-DYNA were performed before the test

to optimize the test's chance of success as well as after the test to calibrate the model (Fig. 29). Once calibrated, the model was used for other impact configurations to obtain the design charts. These charts provide the safe required embedment depth for a given pile, for a given soil strength, and for a given impact condition defined by the truck mass and approaching velocity (Lim, 2011).

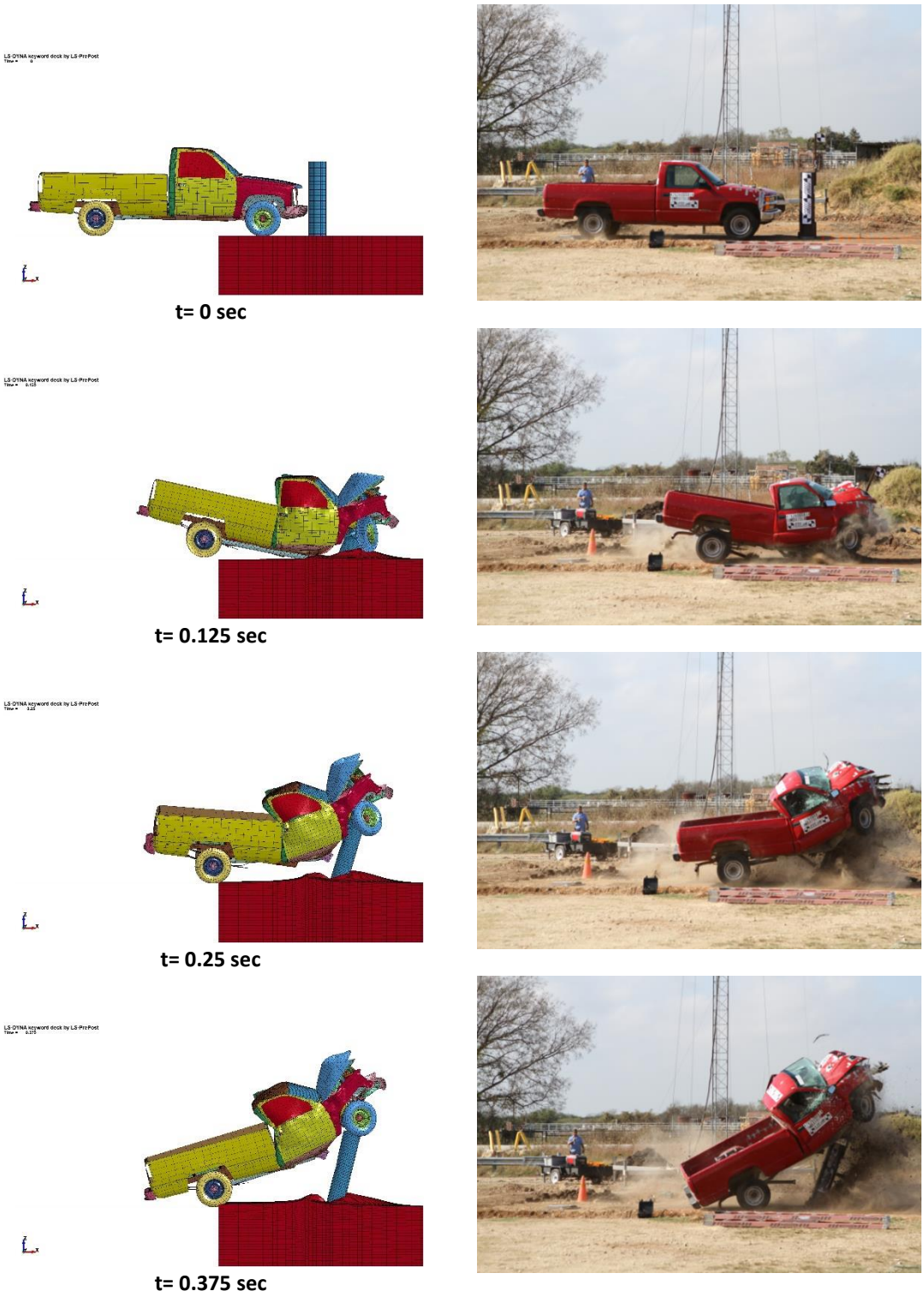


Figure 29. Pickup truck impact test and simulation with LS-DYNA.

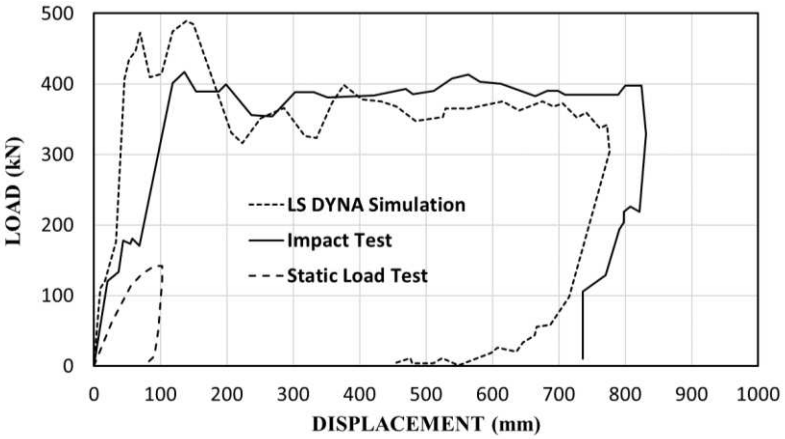


Figure 30. Pile static load and impact load vs. displacement curve.

BIDIRECTIONALLY PRELOADED DRILLED SHAFTS

This 2016 project was sponsored by FHWA/ADSC to evaluate the increase in capacity due to bidirectional preloading and post grouting the bottom of drilled shafts in clay (Loehr et al., 2017). The work was directed and overseen by Erik Loehr of the University of Missouri. Five 0.91 m diameter 10 m long test shafts were installed by drilling under slurry. Shaft TS-2 was the reference shaft with no device at the tip, Shafts TS-1 and TS-3 were equipped with O-Cells at the tip, Shaft TS-4 was equipped with a RIM cell at the tip, and Shaft TS-5 was equipped with a flat jack post grouting device. There was no post grouting of the soil, but simply pre-loading of the bottom of the shafts through various bottom preloading devices.

The testing took place in two stages: preloading, followed by conventional top-down loading. The test shafts were instrumented with strain gages, which gave the load distribution in the shaft during preloading and during top-down loading. During preloading, the O-Cells in TS-1 and TS-3 did not generate significant preloading load (142 kN and 240 kN); this is attributed to the failure of getting concrete to flow beneath the O-Cell during construction. During preloading, the RIM cell generated 534 kN and the post grouting flat jack generated 1023 kN. The load distribution at the end of preloading was similar to the residual load distribution found in driven piles after driving (Briaud Tucker, 1984).

All 5 shafts were then subjected to top-down loading according to the ASTM quick load test procedure. The load settlement curves are shown in Fig. 31. If the results for TS-1 and TS-3 are discounted for the problem explained above, the results indicate some improvement in the shaft performance compared to the reference shaft. For an ultimate load criterion of 10% of diameter, the percent improvement is 6% for the RIM cell and 14% for the post grouting flat jack. This is consistent with the results of the post grouting of drilled shafts project conducted by Synchropile, which gave 14.3% improvement.

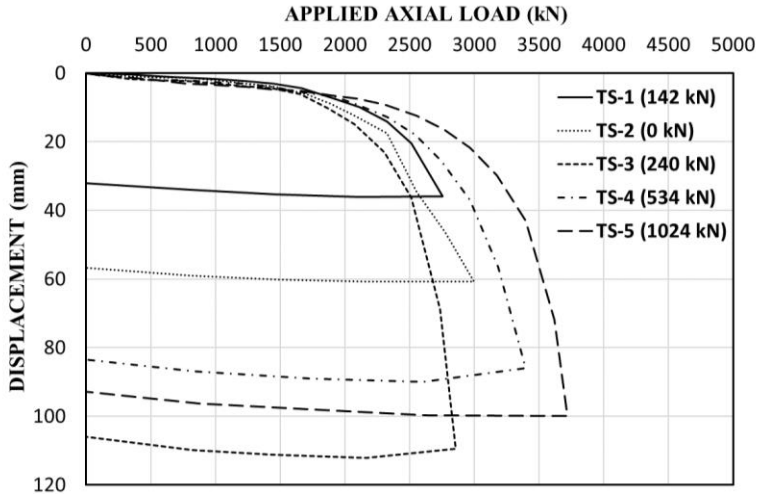


Figure 31. Load settlement curves for the five drilled shafts; the loads in the legend indicate the preloading load (after Loehr et al, 2017).

CONCLUSIONS

40 years of full-scale infrastructure testing at the Texas A&M University National Geotechnical Experimentation Sites have led to a wealth of data and lessons learned, and will continue to serve as a valuable resource for the geotechnical community for many years to come. Some of the conclusions reached from the projects discussed in this paper are as follows. These conclusions are limited to the observations made and to the soil type tested.

1. Reasonable values of K_o are obtained from the early part of the preboring pressuremeter curve. This should be further tested. The step blade measures horizontal pressures, which are the superposition of a penetration test and a lateral expansion test; this leads to high values of K_o.
2. The borehole erosion test is a simple in-situ test to obtain a continuous erodibility profile of soil layers. It is a soil erodibility profiling test, much like the CPT is a strength profiling test.
3. In the stiff to very stiff clay of the NGES, the long-term deflection (205 days) of a horizontally loaded pile was twice the short-term deflection (30-minute load steps). The pressure against the shaft at the ultimate horizontal load matched the pressuremeter limit pressure.
4. The drilled and grouted piles tested exhibited very high values of maximum side friction, a creep movement exponent of 0.02, and a cyclic degradation exponent varying between 0.04 and 0.05; this is limited to the type and amplitude of the cycles performed.
5. Gamma gamma ray logging is the best technique to detect defects in the grout curtain of drilled and grouted piles.
6. Pulling on drilled and grouted piles and on anchors from the bottom leads to higher capacity, stiffer response, less creep vs. time, and less accumulation of cyclic displacement in the site's overconsolidated clay because of post-peak softening and the associated length effect.
7. Drilled and grouted tieback anchors retested 22 years after the initial tests showed a 54% increase in capacity.
8. Non Destructive Techniques (NDT) performed on the top of drilled shafts give a reasonable estimate of the length of drilled shafts but do not give a reliable estimate of defects in drilled shafts. This conclusion is based on tests conducted in 1991, and the technology has evolved significantly since that time; there is a need to repeat such tests to gauge how much progress has been accomplished.
9. Post grouting of a drilled shaft in the stiff clay led to a 15% increase in capacity and stiffness. This was confirmed by another project on bidirectionally preloaded drilled shafts.
10. Soil nails in the stiff clay exhibited a low creep rate at working loads. The creep rate became unacceptable (2 mm per log cycle) only at loads in excess of 80% of the ultimate load.
11. Heating of the soil around geothermal piles leads to an increase in creep rate, while cooling the soil leads to a decrease in creep rate. No change in ultimate capacity was detected.
12. Barriers to contain truck impact around sensitive facilities can be founded on piles with embedment of the order of 2 to 3 m, provided the soil is strong enough. The peak dynamic force measured in one impact test was found to be about 3 times larger than the ultimate capacity of the pile in a static horizontal load test.

ACKNOWLEDGEMENTS

There are many people to thank for the work that has taken place at the National Geotechnical Experimentation Site at Texas A&M University over the last 40 years. They are too numerous to list here in full, but they include the sponsors of the many projects, the students who carried out the work under sometimes very difficult conditions, the colleagues who contributed a helping hand on many occasions, the visitors who brought their projects to the site, and the TAMU administration whose patience for all my requests, sometimes at the last minute, was very appreciated. Special thanks goes to Mohammad Mahdavi for redoing many figures in this article.

REFERENCES

Akrouch, G.A. (2014). *Energy piles in cooling dominated climates*, PhD Dissertation, Zachry Dpt. of Civil Engineering, Texas A&M University, College Station, Texas, USA, 219.

Ballouz, M., Nasr, G., and Briaud, J.-L. (1991). *Dynamic and Static Testing of Nine Drilled Shafts at Texas A&M University Geotechnical Research Sites*, Research Report, Dpt. of Civil Engineering, Texas A&M University, 122.

Bierschwale, M.W., Coyle, H.M., and Bartoskewitz, R.E. (1981). *Field Tests and New Design Procedure for Laterally Loaded Drilled Shafts in Clay*, Report FHWA/TX-81/09+211-3F, Texas A&M Transportation Institute, Texas A&M University System, 129.

Briaud, J.-L. (1997) (a). N*ational Geotechnical Experimentation Sites at Texas A&M University, Clay and Sand: A Summary*, Zachry Dpt. of Civil Engineering, Texas A&M University, College Station, USA.

Briaud, J.-L. (1997) (b). "SALLOP: Simple Approach for Lateral Loads on Piles." *Journal of Geotechnical and Geoenvironmental Engineering*, 123(10), 958-964.

Briaud, J.-L., Ballouz, M., and Nasr, G. (2000). "Static Capacity Prediction by Dynamic Methods for Three Bored Piles." *Journal of Geotechnical and Geoenvironmental Engineering*, 126, (7), 640-649.

Briaud, J.-L., Ballouz, M., and Nasr, G. (2002). "Defect and Length Prediction by NDT Methods for Nine Bored Piles", *Proceedings of the International Deep Foundation Congress*, GSP 116, Orlando, Florida, Geo-Institute, ASCE.

Briaud, J.-L., and Chedid, M. (2015). *The Borehole Erosion Test – BET*, Research Report to the Texas A&M Transportation Institute Intellectual Property Committee, Zachry Dpt. of Civil Engineering, Texas A&M University.

Briaud, J.-L., Chedid, M., Chen, H.C., and Shidlovskaya, A. (2017). "The Borehole Erosion Test." *Journal of Geotechnical and Geoenvironmental Engineering*, ASCE, Reston, Virginia, USA, 143(8).

Briaud, J.-L., and Dupin, R.M. (1990). "Integrity testing of Three Drilled and grouted Piles." *Offshore Technology Conference*, paper OTC 6322, 451-457.

Briaud, J.-L., and Felio, G.Y. (1986). "Cyclic Axial Loads in Piles: Analysis of Existing Data." *Canadian Geotechnical Journal*, 23, (3).

Briaud, J.-L., and Garland, E.E. (1985). "Loading Rate Method for Pile Response in Clay." *Journal of the Geotechnical Engineering Division*, 111, (3).

Briaud, J.-L., and Kubena, M. (1990). *Tension Loading of Two Grouted Piles in Stiff Clay*, Research Report 5885-2, Zachry Dpt. of Civil Engineering, Texas A&M University.

Briaud, J.-L., Powers III, W.F., and Weatherby, D.E. (1998). "Should grouted anchors have short tendon bond length?" *Journal of Geotechnical and Geoenvironmental Engineering*, 124(2).

Briaud, J.-L., and Tucker, L.M. (1984). "Piles in Sand: A Method Including Residual Stresses." *Journal of Geotechnical engineering*, 110(11).

Briaud, J.-L., Tucker, L.M., and Smith, T.D. (1985). "A Pressuremeter Method for Laterally Loaded Piles." *International Conference on Soil Mechanics and Foundation Engineering*, San Francisco.

Chaouch, A., and Briaud, J.-L. (1991). *Pull Out Test on a Drilled and Grouted Pile Loaded from the Top*, Research Report to UNOCAL, Dpt. of Civil Engineering, Texas A&M University, College Station, Texas, USA.

Chaouch, A., and Briaud J.-L. (1992). *Pull Out Test on a Drilled and Grouted Pile Loaded from the Bottom*, Research Report to UNOCAL, Dpt. of Civil Engineering, Texas A&M University, College Station, Texas, USA.

Gan, K.C., and Briaud, J.-L. (1987). *Use of the Stepped Blade in Foundation Design and Comparison with the Pressuremeter*, Research Report 7032, Dpt. of Civil Engineering, Texas A&M University, 451.

Handy, R. L., Remmes, B., Moldt, S., and Lutenegger A.J. (1982). "In Situ Stress Determination by Iowa Stepped Blade." *Journal of the Geotechnical Engineering Division*, 108(11), 1405-1422.

King, P., Fernandez, A., and Pando, M. (2009). "Post Grouted Drilled Shafts – A Comprehensive Case history from Texas." *Proceedings of the 2009 International Foundation Congress and Equipment Exposition*, Geo-Institute, ASCE.

King, P., Fernandez, A., Pando, M.A., Briaud, J.-L., and Magbo, C.C. (2015). *Synchropile Project on Post Grouted Drilled Shafts at Texas A&M University National Clay and Sand Sites*, Research report, Zachry Dpt. of Civil Engineering, Texas A&M University, 42.

Lim, S.G. (2011). *Development of Design Guidelines for Soil Embedded Post Systems using Wide-Flange I-Beams to Contain Truck Impact*, PhD dissertation, Zachry Dpt. of Civil Engineering, Texas A&M University.

Loehr, J.E., Marinucci, A., Hagerty, Duffy, P., Gomez, J., Robinson, H., Day, T., Boeckmann, A., and Cadden, A. (2017). *Evaluation and Guidance Development for Post-Grouted Drilled Shafts for Highways*, Report FHWA-HIF-17-024, Federal Highway Administration, Washington DC, 158 pages.

Mirdamadi, A. (2014). *Deterministic and Probabilistic Simple Model for Single Pile Behavior under Lateral Truck Impact*, PhD dissertation, Zachry Dpt. of Civil Engineering, Texas A&M University.

Murff, J. D. (1980). "Pile capacity in a softening soil." *International Journal of Numerical Analysis Methods in Geomechanics*, 4, 185–189.

Pajouh, M.A. (2015). *Experimental and Numerical Investigation of Impact Loads on a Group of Piles*, PhD dissertation, Zachry Dpt. of Civil Engineering, Texas A&M University.

Powers, W. F., and Briaud, J.-L. (1993). *Behavior of 10 full scale ground anchors installed in stiff clay*, Res. Rep. to Schnabel Found. and the Fed. Hwy. Admin., Dept. of Civ. Engrg., Texas A&M University, College Station, Tex.

Sanchez, M., Briaud, J.-L., Hurlebaus, S., Mahdavi, M., and Bi, G. (2017). *Creep behavior of soil nail walls in high plasticity index (PI) soils*, Report FHWA/TX-15/0-6784-1, Texas A&M Transportation Institute, Texas A&M University System, 440.

The open access Mission of the International Journal of Geoengineering Case Histories is made possible by the support of the following organizations:



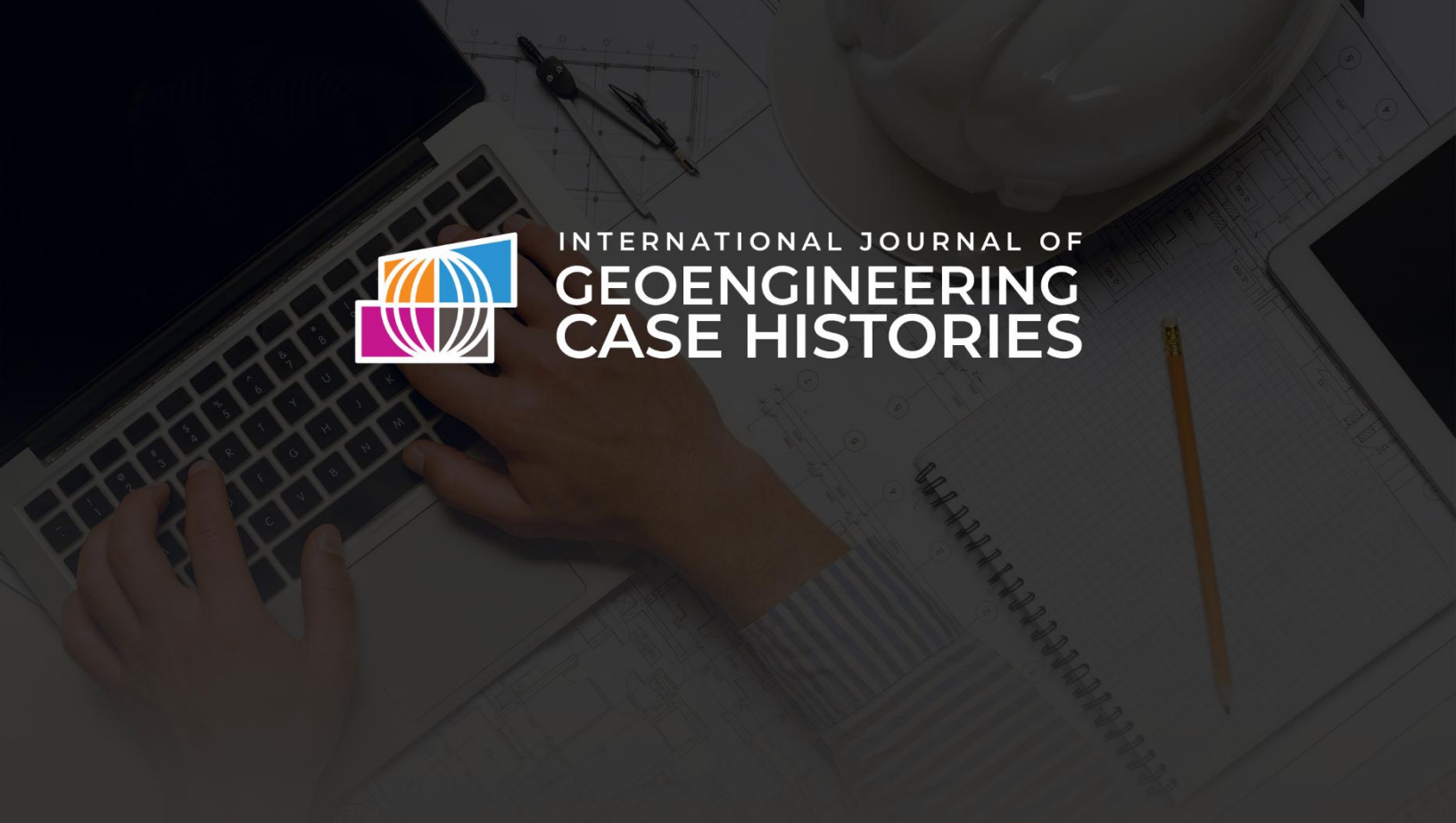








Access the content of the ISSMGE International Journal of Geoengineering Case Histories at:
https://www.geocasehistoriesjournal.org



INTERNATIONAL JOURNAL OF
GEOENGINEERING
CASE HISTORIES

The Journal's Open Access Mission is generously supported by the following Organizations:

dar
a Sidara company

Geosyntec consultants
engineers | scientists | innovators

CONETEC
MUD BAY DRILLING
LANKELMA
Geotech DRILLING

ENGEO
Expect Excellence

Access the content of the ĪSSMGE Īnternational Journal of Geoengineering Case Histories at:
www.geocasehistoriesjournal.org

Downloaded: Friday, November 13 2026, 22:59:06 UTC